

# Adaptive Active Power Sharing Techniques for DC and AC Voltage Control in a Hybrid DC/AC Microgrid

Ángel Navarro-Rodríguez, Pablo García, Ramy Georgious and Jorge García  
Dept. of Electrical, Electronics, Systems & Computers Engineering  
University of Oviedo, LEMUR Group  
Gijón, 33204, Spain

Email: [navarroangel@uniovi.es](mailto:navarroangel@uniovi.es), [garciafpablo@uniovi.es](mailto:garciafpablo@uniovi.es), [georgiousramy@uniovi.es](mailto:georgiousramy@uniovi.es), [garciajorge@uniovi.es](mailto:garciajorge@uniovi.es)

**Abstract**—This paper deals with the AC and DC dynamic voltage control in a hybrid DC/AC Microgrid (MG) with central and distributed Battery Energy Storage Systems (BESSs), applying a power sharing mechanism between the different devices in the MG. The MG is composed by a multiport transformation center and two fixed frequency 3 phase AC Nanogrids (NGs) coupled to a DC bus through 3-phase Power Electronic Converters (PECs). The system pursues to minimize the dependence on the utility grid and the stress in the MGs central BESS, while increasing the power handling capability and the overall system stability during islanding condition. In order to approach the proposed aim, two main concerns are studied in this paper: an adaptive power sharing mechanism between the DC bus and the AC NGs for DC voltage control, and the design and implementation of an AC dynamic local voltage compensator based on Distributed Energy Storage System (DESS). The proposed techniques are validated through simulations and experimental results.

## I. INTRODUCTION

The increasing concern about environmental issues and the rising popularity of concepts as local generation and self-consumption have led to an increasing interest on alternatives to the conventional utility grid as Microgrids (MGs), Nanogrids (NGs) and Smart grids (SGs). Despite its advantages, the weakness and stability problems associated to MGs have been considered since its appearance, demanding significant research interests, specially regarding the power quality improvement [1], [2]. Furthermore, with the appearance of hybrid DC/AC MGs, where distributed energy resources (DERs) and loads may share/draw power in both the AC grid and the DC lines, new MG issues appears as the stability and grid quality in DC and AC [3], [4].

Several topologies for hybrid MGs have been proposed during the last years, classified by the interconnection with the mains and the connection between the DC and the AC

networks [5]. However, most of the examples in the literature are based on a direct connection with the mains in the AC grid and an interlinking converter between the DC and AC buses, being susceptible to contingencies in the mains [3], [4], [6], [7]. In contrast, the MG topology proposed in [8] and shown in Fig. 1, consist in a two-stage completely isolated topology with multiple AC Nanogrids (NGs) that allows to decouple the DC and AC buses from the utility grid through a MG head converter (MGHC). This reduces the impact of distributed generation (DG) in the mains and the sensitivity of the MG to contingencies in the utility grid, being the selected topology for this study. Moreover, the required modification to the already existing infrastructure is minimized, since there are no changes in the distribution system downstream of the transformation center.

Regarding the control system, several control schemes (central controller, master-slave, droop-based control, hybrid approaches ...) are found in the literature to ensure the voltage/frequency control and power sharing in AC distribution networks [6], [9]–[11], and DC grids [12], [13]. In the particular application of hybrid MGs, some control solutions have been proposed [14]. However, most of them are based on a DC/AC interlinking converter operated in grid following mode [3], [4], [6], [7].

Conversely, the topology in [8] is based on DC/AC 3-phase 2-level interlinking converters operated in grid forming mode (slack mode). Compared to droop control strategies, grid forming control methods based on master-slave or multi-slack grid control, with fixed frequency, can simplify the MG design with high presence of DERs interfaced by power electronic converters (PECs), and renewable sources operated under maximum power point tracking (MPPT) [12], [13], [15].

This tight regulation in the interlinking converters, hereinafter referred to as Nanogrid head converters (NGHCs) [8], allows for decoupling the AC from the DC bus dynamics, thus, the NGs behave as CPLs for the LVDC. Counter-intuitive, this might become an issue if the LVDC present a low inertia, for instance during *islanding mode* or under low DC bus capacitance. Therefore, the solution to avoid critical dynamic

---

The present work has been partially supported by the predoctoral grants program Severo Ochoa for the formation in research and university teaching of Principado de Asturias PCTI-FICYT under the grant ID BP14-135. This work also was supported in part by the Research, Technological Development and Innovation Program Oriented to the Society Challenges of the Spanish Ministry of Economy and Competitiveness under grant ENE2016-77919-R and by the European Union through ERFD Structural Funds (FEDER).

and stability issues relies on making the NGHCs participate on the regulation of the LVDC, involving a dynamic power sharing between DC and AC buses. However, the dynamic power sharing between DC and AC buses in a hybrid MG when the coupling converters are operated in slack mode, is not yet exploited. In [16], an study on cascaded converters stability is carried out, presenting an analogous problem. A power balancing mechanism between AC and DC using a  $V_g/V_{dc}$  droop is also proposed in [17]. However, the first method is related to a pure DC MG while the second is implemented in AC/DC/AC grid tied converters operated in droop-based grid feeding. The aim of the present study is to implement a dynamic sharing mechanism to the MG under study.

Concerning the dynamic voltage control and active power sharing in AC grids, many studies can be found in the literature based on the variation of the frequency with the active power (P/f), being the stiffness determined by the system inertia [18]–[22]. However, when the fixed frequency approach is used instead, active power variations will affect mainly the voltage magnitude (P/V) being the grid inertia dependent on the grid equivalent capacitance as in DC grids [23]. In addition, the high presence of PECs, that reduces the system inertia, and the challenges imposed by the high presence of constant power loads (CPLs) [16], make the grid prone to stability and dynamic response issues. The concepts of Quadratic Voltage Control (QVC) and virtual capacitance, studied in [23], seems to be a promising solution to this problems applicable in both DC and AC.

In summary, this paper deals with the AC and DC voltage control in a hybrid DC/AC MG considering central and distributed Battery Energy Storage Systems (BESSs), which topology is based on the MG presented in [8]. A power sharing mechanism between the AC NGs and the DC bus is proposed. The system will have as main constraints the reduced dependency on the utility grid (mains), the islanded operation and the optimization of the ESS usage. The main contributions are related with the two main concerns that are studied: 1) the design of an adaptive method for the dynamic power sharing between the DC bus and the AC NGs for an enhanced DC voltage control, improving the overall MG performance; and 2) the implementation of an AC voltage compensator for the NG-based distribution system. The compensation will rely on the use of virtual capacitor for an improved system stiffness.

This paper follows the study presented in [24]. The changes incorporated respect to the conference paper are the improvement of the adaptive power sharing algorithm and the experimental verification of the proposed methods. The paper is organized as follows. Section II introduces the hybrid DC/AC Microgrid topology under study. Section III explains the basics of the proposed voltage control loops in DC and AC systems. Section IV covers the proposed adaptive voltage control in the hybrid DC/AC MG. Section V presents the simulation and experimental results. Section VI contains the dynamic characterization of the system through the frequency response

analysis. Finally, section VII states the conclusions.

## II. SYSTEM DESCRIPTION AND ANALYSIS

The hybrid MG under study, shown in Fig. 1, is based on the topology presented in [8], and is composed by a MG transformation center (MGTC) and two 3-phase AC NGs based on fixed frequency Master-Slave topology. The MGTC consists of a central BESS (battery + DC/DC converter) and a connection to the mains interconnected by a common Low Voltage DC bus (LVDC) to two NG Head Converters (NGHCs) feeding the AC NGs. The BESS and the mains are interfaced with the LVDC by a three-port solid-state transformer (SST). Likewise, the mains are interfaced with the SST by means of an AC/DC MG head converter (MGHC). It is worth to point out that the SST operation is out of the scope of this paper, considering it as an ideal connection that provides galvanic isolation. The MG is designed as follows. The NGHC acts as a slack, both for the AC voltage magnitude and frequency. The MGs loads, constant power loads (CPLs) and Constant Impedance Loads (CILs), are only located at the 3 phase NGs. Under this configuration, the load as seen by the LVDC is drawn by the NGHCs. Additionally, different distributed resources such as Distributed Generation (DG) and ESSs can be installed at NG level. A central controller governs the MGTC and low bandwidth communications are considered in the NGs between the DGs, ESSs and NGHCs. The central BESS and the MGHC connected to the mains are operated in power control mode, receiving commands from the central controller.

Power mismatches in conventional grids are absorbed by the high inertia of generators. However, in the case under study, they have to be supported by the energy storage elements, including capacitances, installed at the MG. As a first approach, DGs and DESS in the NG will operate with constant PQ commands while the slack NGHCs will absorb the power transients, controlling the voltage magnitude and frequency. Additionally a local dynamic voltage compensator able to share active power might be considered in the NGs ( $P_{vc}$ ). Depending on the MG being connected/disconnected to the main grid, two modes of operation are defined: 1) During *non-islanding* operation, the mains  $P_{mains}$  and the BESS  $P_{BESS}$  can share the effort; 2) During *islanding*, the MG is disconnected from the utility grid and only the BESS is available as a power source in the transformation center.

In any case, the voltage in DC and AC NGs should remain under control within regulation limits. Additionally, two constraints are established: 1) The dependence on the utility grid should be minimized; 2) The BESS limitations (bandwidth, available power, State of Charge (SoC)) have to be considered in the power sharing. This paper is focused on the operation during *islanding* mode.

Although the DGs in the NG could be used to provide ancillary services, most of DERs in the NG either present a low response or should be operated in Maximum Power Point Tracking (MPPT). However, DESSs in the NG can be used, providing local compensation while reducing the conduction

$$\frac{d}{dt} \begin{bmatrix} i_{i^k d} \\ v_{g^k d} \\ i_{i^k q} \\ v_{g^k q} \end{bmatrix} = \begin{bmatrix} \frac{-R_k}{L_k} & \frac{1}{L_k} & 0 & 0 \\ \frac{1}{C_k} & 0 & 0 & 0 \\ 0 & 0 & \frac{-R_k}{L_k} & \frac{1}{L_k} \\ 0 & 0 & \frac{1}{C_k} & 0 \end{bmatrix} \begin{bmatrix} i_{i^k d} \\ v_{g^k d} \\ i_{i^k q} \\ v_{g^k q} \end{bmatrix} + \begin{bmatrix} \omega_{e^k} & 0 \\ 0 & \omega_{e^k} \\ 0 & 0 \\ 0 & 0 \end{bmatrix} \begin{bmatrix} i_{i^k d} \\ v_{g^k d} \\ i_{i^k q} \\ v_{g^k q} \end{bmatrix} + \begin{bmatrix} \frac{1}{L_k} & 0 & 0 & 0 \\ 0 & \frac{-1}{C_k} & 0 & 0 \\ 0 & 0 & \frac{1}{L_k} & 0 \\ 0 & 0 & 0 & \frac{-1}{C_k} \end{bmatrix} \begin{bmatrix} v_{g^k d} \\ i_{g^k d} \\ v_{g^k q} \\ i_{g^k q} \end{bmatrix} \quad (1)$$

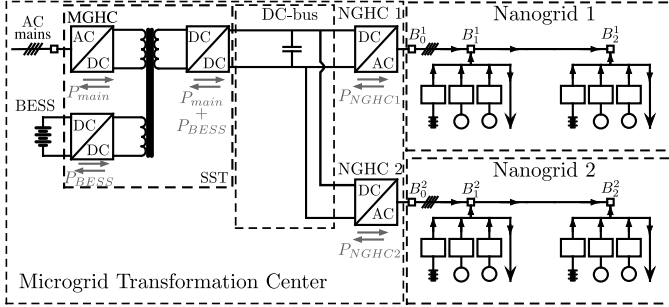


Fig. 1. Topology of the Hybrid DC/AC Microgrid under study.

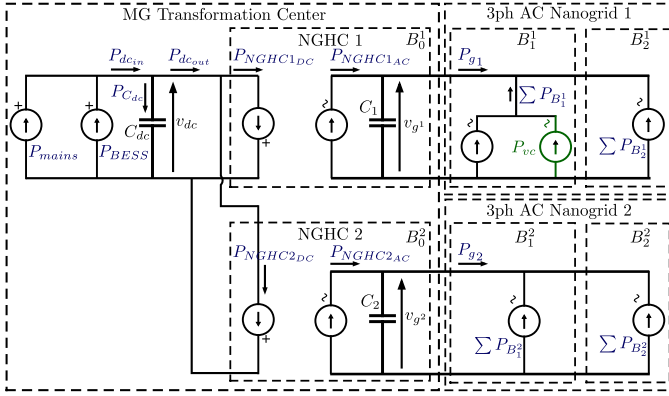


Fig. 2. Simplified power sharing scheme within the Hybrid DC/AC MG.

losses. As a first approach, in this study one local ESSs will be used for transient compensation located at the first node of NG1 ( $B_1^1$ ). Fig. 2 shows a simplified scheme of the MG illustrating the different elements participating on the power sharing, where  $\sum P_{B_j^k}$  ( $k$  denotes the NG, while  $j$  the node) is the total power share between DGs, DESS and active power loads within a node,  $\sum P_{B_j^k} = \sum (P_{DG_j^k} + P_{DESS_j^k} - P_{L_j^k})$ .

The system model for the voltage control, both in AC and DC, is simplified to a capacitor, neglecting line impedances and approximating the current control loops of the PECs to a low-pass filter. 3-phase balanced AC NGs are assumed.

The modeling of the system under study will be based on the simplified power scheme for one of the NGHCs shown in Fig. 3. Thus, the AC system modeled in  $dq$  synchronous reference frame is defined by (1), where  $k$  is the NG identifier,  $v_{g^k}$  is the NG voltage at node  $B_0^k$ ,  $i_{i^k}$  is the current drawn by the NGHCs into the NGs (i.e. the control action of NGHCs),  $\omega_{e^k}$  is the grid frequency and  $i_{g^k}$  is the total current drawn by the buses  $B_1^k$  and  $B_2^k$ , i.e., the system disturbance.

The DC link can be modeled in terms of active power as (2),

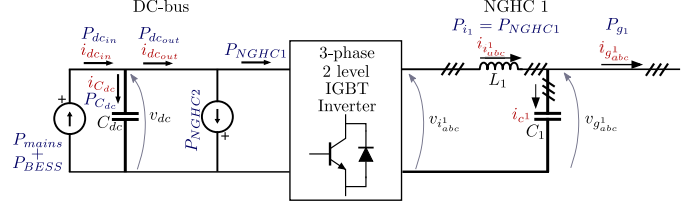


Fig. 3. Simplified equivalent power scheme of one of the NGHCs.

where  $C_{dc}$  is the LVDC capacitor,  $P_{dcin}$  is the power shared by the main and the central BESS, and  $P_{dcout}$  is the power drawn by the NGHCs ( $P_{dcout} = P_{NGHC1}(t) + P_{NGHC2}(t)$ ), being defined by (3) and (4), assuming  $v_{gq} = 0$ . Thus, the NGHCs are seen as CPLs by the DC link. The power flowing into the capacitor is defined as  $P_{C_{dc}} = P_{dcin} - P_{dcout}$ .

$$\frac{dv_{dc}(t)}{dt} = \frac{1}{C_{dc}v_{dc}(t)} \left( P_{dcin}(t) - \underbrace{(P_{NGHC1}(t) + P_{NGHC2}(t))}_{P_{dcout}} \right) \quad (2)$$

$$P_{dcout}(t) = \sum_{k=1}^2 P_{NGHC_k}(t) \quad (3)$$

$$P_{NGHC_k}(t) = \frac{3}{2} \left( v_{g_d^k}(t) i_{i_d^k}(t) + v_{g_q^k}(t) i_{i_q^k}(t) \right) \quad (4)$$

### III. VOLTAGE CONTROL: CONTROLLER DESIGN

The MGTC control will involve the dynamic control of both DC link and AC NGs voltages. The closed loop voltage controllers, both in AC and DC, will be based on a feedback PI regulator, implemented in  $dq$  synchronous reference frame in the case of the AC NGs. Two alternatives for the basic voltage control are considered in this paper, following the analysis and discussion proposed in [23]. Fig. 4 shows the generic representation of those alternatives for DC voltage control (or each of the axis of the  $dq$  synchronous reference frame voltage control), where  $i_{L(t)}$ ,  $p_{L(t)}$  and  $g_{L(t)}$ , are the time dependent disturbances drawn by constant current loads (CCLs), constant power loads (CPLs) and constant impedance loads (CILs) respectively. It is necessary to point out that  $g_{L(t)}$  is the conductance that represents the inverse of the real part of a CIL. According to this, the system plant is defined by (5), being a non-linear system.

$$\frac{dv(t)}{dt} = \frac{1}{C} \left( i(t) - \underbrace{\left( i_{L(t)} + \frac{p_{L(t)}}{v(t)} + g_{L(t)}v(t) \right)}_{Disturbance} \right) \quad (5)$$

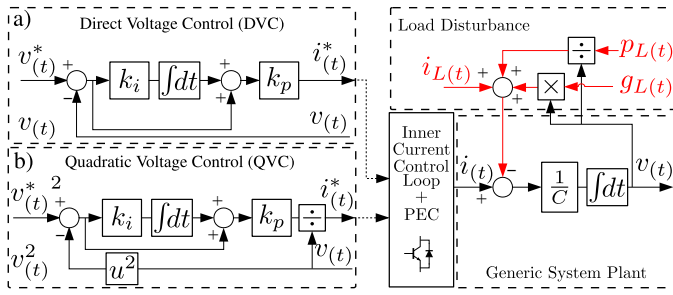


Fig. 4. Voltage control schemes, based on cascaded control. a) Direct Voltage Control (DVC); b) Quadratic Voltage Control (QVC).

Pursuant to this expression, the conventional voltage control, referred in [23] as Direct Voltage Control (DVC), will present a non linear behavior under the presence of CGLs and CPLs. Alternatively, Quadratic Voltage Control (QVC) can be used instead. Although it has been proposed before in the literature referred as energy based controller, its applications has been limited to the DC link control of DC/AC converters [25], [26]. Nonetheless, its application can be generalized to any cascade-based voltage control as slack converters in both DC and AC MGs. It is worth to point out that this assumption is valid provided that the inner power and current control loops, including the converter and current filter, behave as an ideal  $2^{nd}$  order low-pass filter with a much higher bandwidth than the outer voltage control loop. The details for its implementation in AC are given later in this section. The QVC generic expression is defined in (6).

$$P_{(t)}^* = k_p \left( (v_{(t)}^*)^2 - v_{(t)}^2 \right) + k_i \int (v_{(t)}^*)^2 - v_{(t)}^2 dt \quad (6)$$

Where  $k_p$  and  $k_i$  are the ideal PI regulator gains.

Despite the fact that the QVC also presents a non-linear relation between the voltage and the load disturbance, the relation between the square voltage and the CPLs is linear considering the system plant in (7), where  $P^*$  is the control action and  $P_{C(t)}$  is the power flowing into the capacitor.

$$v_{(t)} \frac{dv_{(t)}}{dt} = \frac{1}{C} P_{C(t)} \Rightarrow \frac{dv_{(t)}^2}{dt} = \frac{2}{C} P_{C(t)} \quad (7)$$

The main feature of the voltage control for the application presented in this paper is the disturbance rejection capability. In order to analyze how the disturbance rejection of each method is affected by the type of load, their disturbance to output transfer functions were obtained and analyzed in [23]. The expressions for the DVC are shown in (8), (9) and (10).

$$\frac{\Delta V(s)}{\Delta I_L(s)} \approx \frac{-sV_0^2}{s^2V_0^2C + s(k_pV_0^2 - P_{L0} + G_{L0}V_0^2) + k_ik_pV_0^2} \quad (8)$$

$$\frac{\Delta V(s)}{\Delta P_L(s)} \approx \frac{-sV_0}{s^2V_0^2C + s(k_pV_0^2 - P_{L0} + G_{L0}V_0^2) + k_ik_pV_0^2} \quad (9)$$

$$\frac{\Delta V(s)}{\Delta G_L(s)} \approx \frac{-sV_0^3}{s^2V_0^2C + s(k_pV_0^2 - P_{L0} + G_{L0}V_0^2) + k_ik_pV_0^2} \quad (10)$$

Where  $V_0$ ,  $P_{L0}$  and  $G_{L0}$  are the voltage magnitude, the CPL level, and the CIL level at the equilibrium point respectively.

The expressions for the QVC are stated in (11), (12) and (13), where  $I_{L0}$  is the CCL level at the equilibrium point.

$$\frac{\Delta V(s)}{\Delta I_L(s)} \approx \frac{-sV_0}{s^2V_0C + s(2k_pV_0 + I_{L0} + 2G_{L0}V_0^2) + 2k_ik_pV_0^2} \quad (11)$$

$$\frac{\Delta V(s)}{\Delta P_L(s)} \approx \frac{-s}{s^2V_0C + s(2k_pV_0 + I_{L0} + 2G_{L0}V_0^2) + 2k_ik_pV_0^2} \quad (12)$$

$$\frac{\Delta V(s)}{\Delta G_L(s)} \approx \frac{-sV_0^2}{s^2V_0C + s(2k_pV_0 + I_{L0} + G_{L0}V_0^2) + 2k_ik_pV_0^2} \quad (13)$$

These expressions demonstrate a clear dependence of the disturbance to output transfer functions on the CPL, CIL and CCL levels in both the DVC and QVC. However, the DVC presents a critical negative dependency on CPL level,  $P_{L0}$ , for any kind of load disturbance, which can compromise the system stability. On the contrary, the QVC eliminates the dependency on CPL level. Fig. 5 shows an example of system response comparing the DVC and QVC under the same conditions, for different CPL levels at the equilibrium point  $P_{L0}$ , assuming  $I_{L0} = 0A$  and  $G_{L0} = 0\Omega^{-1}$ . As shown, the DVC response is worsen as  $P_{L0}$  increases, decreasing its gain margin, tending to instability, while the QVC response remains constant.

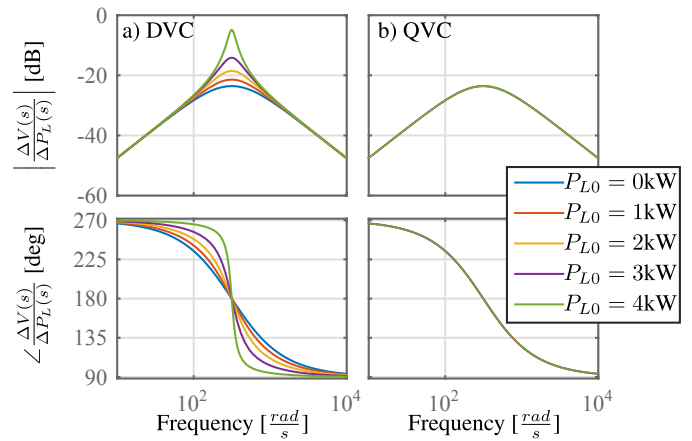


Fig. 5. Bode diagram of the CPL disturbance to output transfer function  $\frac{\Delta V(s)}{\Delta P_L(s)}$  for different values of  $P_{L0}$ , assuming  $I_{L0} = 0A$  and  $G_{L0} = 0\Omega^{-1}$ . a) DVC response, b) QVC response. The parameters for both are:  $V_0 = 300V$ ,  $\zeta = 1$ ,  $\omega_n = 2\pi 50 \frac{rad}{s}$ .

Further analysis and comparison of DVC and QVC are provided in [23]. Due to the high presence of PECs, CPLs and constant power generation expected in the grid under analysis,

a control based on the QVC is proposed for the application presented in this paper.

In order to tune the voltage regulator, a tuning method based on the linearized reference tracking transfer function is used. Applying linearization, the close loop system defined by (6) and (7) can be approximated as (14), where  $V_0^*$  and  $V_0$  are the voltage reference and the voltage in the equilibrium point respectively. Considering operation near the equilibrium point and  $V_0^* = V_0$ , (14) can be approximated by a second order system with a determined natural frequency  $\omega_n$  and a damping factor  $\zeta$  as (15). Thus, the PI regulator parameters of QVC are tuned according to (16). The units of  $k_p$  and  $k_i$  are  $[\Omega^{-1}]$  and  $[s^{-1}]$  respectively, behaving the PI as an admittance. The natural frequency  $\omega_n$ , should be selected according to the cascaded control premises, while the damping factor,  $\zeta$ , can be selected as a trade-off between overshoot and settling time.

$$\frac{V(s)}{V_0^*} \approx \frac{s2k_p V_0^* + 2k_p k_i V_0^*}{s^2 C V_0 + s2k_p V_0 + 2k_p k_i V_0} \quad (14)$$

$$\frac{V(s)}{V_0^*} \approx \frac{2\zeta\omega_n s + \omega_n^2}{s^2 + 2\zeta\omega_n s + \omega_n^2} \quad (15)$$

$$k_p = \zeta\omega_n C; \quad k_i = \frac{\omega_n^2 C}{2k_p} \quad (16)$$

#### A. QVC applied to the LVDC voltage control

The described QVC scheme can be applied directly as shown in 4(b), considering the control action of the PI regulator as the active power reference required by the DC bus capacitor. The specific basic DC bus voltage control is shown in Fig. 6.

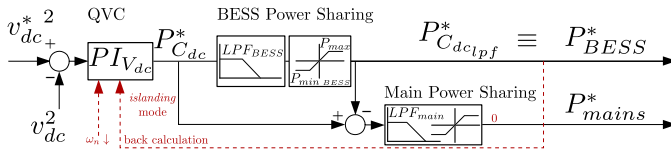


Fig. 6. DC bus slack controller based on Quadratic Voltage Control. *islanding* mode modifications highlighted in red.

As specified before, during *non-islanding* both the BESS and the main grid participate in the control. To reduce the dependence on the main grid, the BESS provides the low bandwidth variations, within its power limitations, while the main contribute with the high bandwidth transients unless the battery power is limited for any reason, in which case the main will participate also in the steady state. In the case of *islanding*, the battery would be the only available power source to maintain the regulation of the DC link. In that case, to maintain the proper operation of the voltage regulator, either a back calculation or a reduction on the control bandwidth,  $\omega_n$ , should be applied to fulfill the cascaded control requirements.

#### B. QVC applied to the 3-phase AC voltage control

The QVC can be applied to the 3-phase AC control considering the following assumptions:

- If the control is implemented in the  $dq$  synchronous reference frame, and assuming the system plant (3-phase capacitor) is balanced and decoupled cross-coupling terms in the control scheme, voltage control loop can be defined by two independent DC systems one for  $d$ -axis and another for the  $q$ -axis.
- The scaling factor of the  $dq$  reference frame,  $\frac{3}{2}$  in the case of using magnitude conservative transformation, should be considered.
- The active power is calculated as a sum of a  $d$ -axis power component,  $P_d$ , and  $q$ -axis power component  $P_q$ , according to the general expression in (17), considering the term  $P_q \ll P_d$ .

$$P(t) = \underbrace{\frac{3}{2}v_d(t)i_d(t)}_{P_d} + \underbrace{\frac{3}{2}v_q(t)i_q(t)}_{P_q} \quad (17)$$

Under these assumptions, the differential equation for the plant can be simplified as (18).

$$\frac{dv_{g_x^k}(t)}{dt} = \frac{1}{C_k} \left( i_{i_x^k}(t) - \underbrace{\left( i_{L_x^k}(t) + \frac{2}{3} \frac{P_{L_x^k}(t)}{v_{g_x^k}(t)} + g_{L_x^k}(t)v_{g_x^k}(t) \right)}_{\text{Disturbance } i_{g_x^k}} \right) \quad (18)$$

Where  $x$  indicates the reference frame  $d$ -axis or  $q$ -axis. Under a balanced load  $g_{L_x^k}$  is assumed to be the same in the  $d$ -axis and  $q$ -axis.

The PI expression for the QVC in (6) is also modified by (19) for the AC  $dq$  implementation.

$$\frac{2}{3}P_{x(t)}^* = k_p \left( (v_{x(t)}^*)^2 - v_{x(t)}^2 \right) + k_i \int (v_{x(t)}^*)^2 - v_{x(t)}^2 dt \quad (19)$$

The PI parameters  $k_p$  and  $k_i$  are tuned as in the DC application (16). It is worth noting that under the described assumptions, the expressions (8)-(13) are also valid for each of the  $dq$  axis substituting  $P_{L0}$  by  $\frac{2}{3}P_{L0}$  and  $\Delta P_L$  by  $\frac{2}{3}\Delta P_L$ .

Considering all the above, a voltage control in the  $dq$  reference frame is proposed based on QVC and fixed frequency. The complete cascaded control scheme for a 3-phase AC slack converter is shown in Fig. 7. A grid current decoupling term could be added in order to improve the disturbance rejection, drawn in green color. However, an improved disturbance rejection could increase the stress in the DC side for the proposed MG topology, which is translated in an increased stress in the BESS during an *islanding* scenario.

#### IV. HYBRID DC/AC VOLTAGE CONTROL

The proposed hybrid MG should maintain the power quality and reliability in both the LVDC bus and the AC NGs. This paper deals with the specific task of managing the dynamic

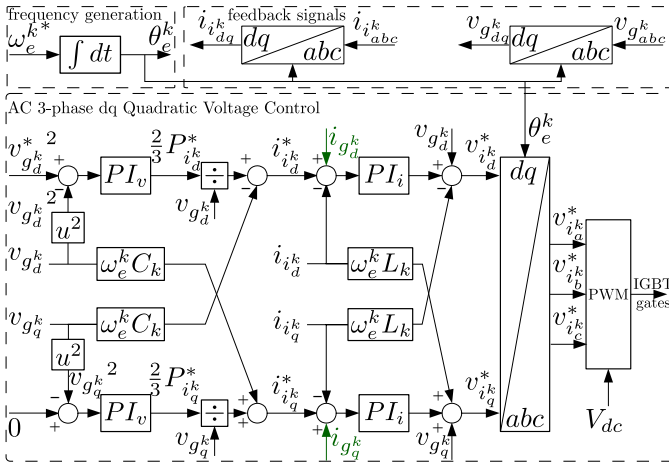


Fig. 7. NGHCs basic AC slack controller based on AC quadratic voltage control implemented in the  $dq$  reference frame.

active power sharing between the elements present in the grid in order to keep the voltage magnitude quality, and the frequency in the case of the AC NGs. The proposed power topology allows to decouple the events and contingencies happening in the LVDC bus from the voltage control in the NGs, as long as the DC voltage remains within certain levels. However, the NGHCs control is not decoupled from the LVDC, being the last one subjected to any disturbance taking place in the NGs. During *islanding*, this control scheme leads to the battery and the DC link capacitor absorbing/injecting any power mismatch within the NGs. In order to soften this effect a coupled hybrid control is proposed as follows.

#### A. The DC bus voltage control scheme

The proposed DC bus voltage control scheme is defined as shown in Fig. 8. It consists on a QVC controller generating a power reference  $P_{C_{dc}}^*$ . In order to limit the stress on the central BESS and comply with its limitations (bandwidth or instantaneous power),  $P_{C_{dc}}^*$  is divided into a low ( $P_{C_{dc1pf}}^*$ ) and high ( $P_{C_{dc2hpf}}^*$ ) bandwidth components by using low pass filters and saturation. The low frequency command  $P_{C_{dc1pf}}^*$  will be given by the BESS, whereas the  $P_{C_{dc2hpf}}^*$  command will be share by the utility grid (if available) and the NGHCs,  $P_{NGHC_k}^*$ . As *islanding* mode is assumed in this paper, the utility grid power command  $P_{main}^* = 0$ . It is worth noting that adjusting the power drawn by the NGHCs by commanding a  $P_{NGHC_k}^*$  will lead to an adverse effect in the AC NGs voltage controller, being necessary to pursue for a trade-off between the DC and AC NGs quality based on the conditions of each NG.

#### B. Adaptive NGs power sharing algorithm

The power shared between the NGHCs will be defined by an adaptive algorithm consisting in the use of complementary sharing coefficients, calculated based on DC bus and AC NGs instantaneous conditions. An initial approach was proposed in

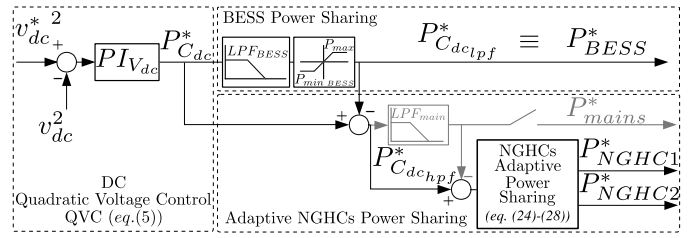


Fig. 8. Proposed hybrid DC/AC voltage control: DC voltage control scheme based on adaptive power sharing between the different elements in the MG transformation center.

[24] consisting of a local NGHC coefficient calculation, (20), and a normalization process.

$$\sigma_k(t) = k_{ish} \int \lambda_{dc}^k \Delta v_{dc_{pu}}(t) - \lambda_g^k \Delta v_{g^k_{pu}}(t) dt \quad (20)$$

$$\Delta v_{dc_{pu}}(t) = \frac{v_{dc}(t) - v_{dc}^{ss}(t)}{v_{dc}^{ss}(t)} \quad (21)$$

$$\Delta v_{g^k_{pu}}(t) = \frac{|v_{g^k}(t)| - |v_{g^k}^{ss}(t)|}{|v_{g^k}^{ss}(t)|} \quad (22)$$

Where  $v_{dc}^{ss}$  and  $|v_{g^k}^{ss}|$  are the steady-state values of DC voltage and AC voltage magnitude, i.e., the values at the equilibrium point, and  $|v_{g^k}|$  is the AC voltage magnitude define as (23).

$$|v_{g^k}| = \sqrt{v_{g_d^k}^2 + v_{g_q^k}^2} \quad (23)$$

The coefficients for each NGHC,  $\sigma_k$ , were obtained for each NGHC as a function of the DC bus and AC NGs voltage variations in p.u.,  $\Delta v_{dc_{pu}}$  and  $\Delta v_{g^k_{pu}}$ , defined in (21) and (22). Two constant weighting factors,  $\lambda_{dc}^k$  and  $\lambda_g^k$ , allow to modify the importance of each voltage variation, while the integral gain  $k_{ish}$  determines the adaptation speed.

The continuous integration in this method allows for fast and continuous adaptation. However, the fast adaptation might interferes with the system dynamics, and it requires a high bandwidth at the communication link used for the exchange of the coefficients. Moreover, as the variable  $\Delta v_{dc_{pu}}$  is the same in the calculation of the coefficient for both NGHCs, its dependency can be avoided as long as  $\lambda_{dc_k}$  is the same for both NGHCs. Thus, the adaptation algorithm has been modified for the studied application in this paper. The algorithm consists on the following steps:

1) *Transient Detection*: The sharing coefficients will be updated when a significant active power disturbance is demanded to the Hybrid MG leading to an asynchronous update of those coefficients. For that purpose, a transient detection scheme is proposed. As in the proposed MG any active power change will have an impact in the LVDC, the DC bus voltage will be the signal used for determining the transient state. In order to obtain the transient window, a transient detection method, based on the presented in [22], is proposed for its application



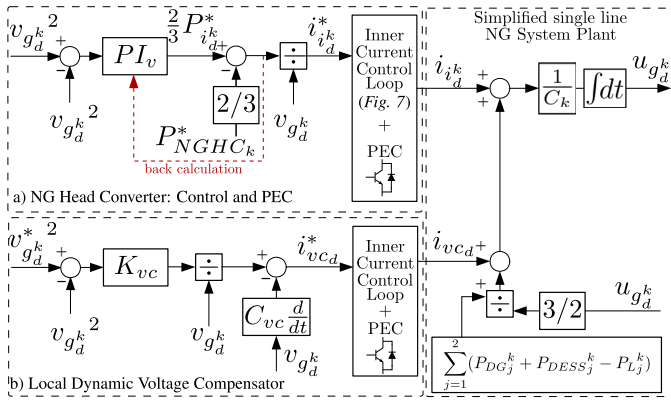


Fig. 10. Proposed hybrid DC/AC voltage control: decentralized AC NGs voltage control scheme. a) NGHC control; b) Local voltage compensator.

control topology for the local dynamic voltage compensator is shown in Fig. 10b) and defined by (29). A virtual capacitance ( $C_{vc} \frac{d}{dt}$ ) increases the grid equivalent capacitance, enhancing the initial transient response and improving the participation during transients in the hybrid sharing mechanism. A low pass filter is needed in the practical implementation of the derivative term. A P quadratic regulator ( $K_{vc}$ ) improves the grid voltage damping, and enable the participation during steady state in the hybrid DC/AC power sharing during abnormal conditions, for instance, if the central BESS is overloaded during *islanding*. Both parts of the controller can be implemented independently or combined depending on the limitations of the DG or DBESS providing that service.

$$i_{vc,dq}^* = \underbrace{\frac{K_{vc,dq} \cdot (v_{g,dq}^*(t)^2 - v_{g,dq}^k(t)^2)}{v_{g,dq}^k(t)}}_{\text{damping factor}} - \underbrace{C_{vc} \cdot \frac{d}{dt} v_{g,dq}^k(t)}_{\text{Virtual Capacitor}} \quad (29)$$

## V. SIMULATION AND EXPERIMENTAL RESULTS

The proposed system has been validated through simulations in MATLAB/Simulink<sup>®</sup> and experimentally in a Hybrid DC/AC MG full scale prototype implemented within the facilities of the research group *Laboratory for Electrical Energy Management Unified Research* in the University of Oviedo, Spain. The system parameters are summarized in Table I, valid for both the simulation and the experimental setup. Two scenarios are consider to evaluate the performance of the control topology proposed in this paper compared with the *base case* operation. The first scenario consists on applying the proposed adaptive technique for power sharing without local AC voltage compensation. In the second scenario, a local voltage compensator is activated in the  $NG_1$ . Considering the increasing penetration of CPLs and their negative effect in the system stability and dynamic response [12], [23], the system has been evaluated under CPLs, considering them as the most critical disturbance when compared with CILs and CCLs.

The *base case* consists in the operation when the control schemes presented in Fig. 8 and 10 are used, by disabling the

TABLE I  
SIMULATION AND EXPERIMENTAL SYSTEM PARAMETERS

AC Nanogrids Parameters	Values
AC Nominal Voltage ( $V_{g1}^*$ , $V_{g2}^*$ )	212 $V_{AC,rms}$ / 50 Hz
NGHCs AC inner control loop BW	$2\pi 500$ rad/s
NGHCs AC voltage control $\omega_n / \zeta$	$2\pi 37.5$ rad/s / 2
NGHCs Filter Capacitor ( $C_1$ , $C_2$ )	80 $\mu F$
NGHCs Filter Inductance ( $L_1$ , $L_2$ )	1 mH
NGHCs rated power	50 kVA
AC voltage compensator gains $K_{vc} / C_{vc}$	$0.2 / 5 \cdot 10^{-4}$
AC voltage compensator BW	2 $\pi$ 500 rad/s
AC CPL current control BW	2 $\pi$ 500 rad/s
DC link and adaptive power sharing	Values
DC Nominal Voltage ( $V_{dc}^*$ )	700 V
DC inner control loop BW	2 $\pi$ 500 rad/s
DC equivalent Capacitor ( $C_{dc}$ )	1100 $\mu F$
DC Voltage control loop $\omega_n / \zeta$	2 $\pi$ 50 / 1
Central BESS BW / $P_{max}$	75 Hz / 8.5 kW
Power Sharing $\lambda_g^1 / \lambda_g^2 / \delta_{max} / \eta_m$	1 / 1 / 0.5 / 2
Transient detection $T$ / threshold	2 ms / $5 \cdot 10^{-3}$

power sharing in DC ( $\sigma'_1 = \sigma'_2 = 0$ ) and without local voltage compensation in the NGs. Considering a BESS bandwidth of 75Hz, in the base case the DC voltage control bandwidth is reduced to 10Hz in order to comply with the cascaded control requirements for stability reasons.

On the other hand, when the proposed technique is applied, the overall inner control loop bandwidth is assumed to be 500Hz thanks to the NGHCs participation, and the DC voltage controller bandwidth can be increased up to 50Hz.

### A. Simulation Results

The simulation results are shown in Fig. 11, where the *base case* and the proposed method are compared. It shows the DC voltage, the AC voltage in both NGs in p.u., the sharing coefficients  $\sigma'_k$  and the transient window used for updating the coefficients, the power commands generated by the DC controller in Fig. 8 and the CPL in each NG. The system is tested under multiple steps of CPL disturbances in both NGs. The sequence of events for the proposed method is as follows:

- Between  $t = 0s$  and  $t = 0.25s$ , the proposed sharing technique and the local AC voltage compensator are inactive. The effect of using excessive voltage control bandwidth with reduced inner control bandwidth is illustrated.
- At  $t = 0.25s$ , the proposed sharing technique is activated. As expected, the power required by the DC voltage controller is now shared between both NGs and central BESS, reacting one NG to the events on the other. As the BESS provides the steady state, the power shared operates only during the transients. The DC voltage transients are improved compared to the *base case*, however the AC NGs voltages are distorted as a consequence.
- At  $t = 0.65s$ , a local voltage compensator in  $B_1^1$  ( $NG_1$ ) is activated. This leads to an overall improvement in both DC and AC voltages reducing significantly the voltage variations under CPL steps.
- At  $t = 1.3s$ , the total system load exceeds the central BESS maximum power, leading to an overall MG collapse for the *base case* at  $t = 1.5s$ . On the other

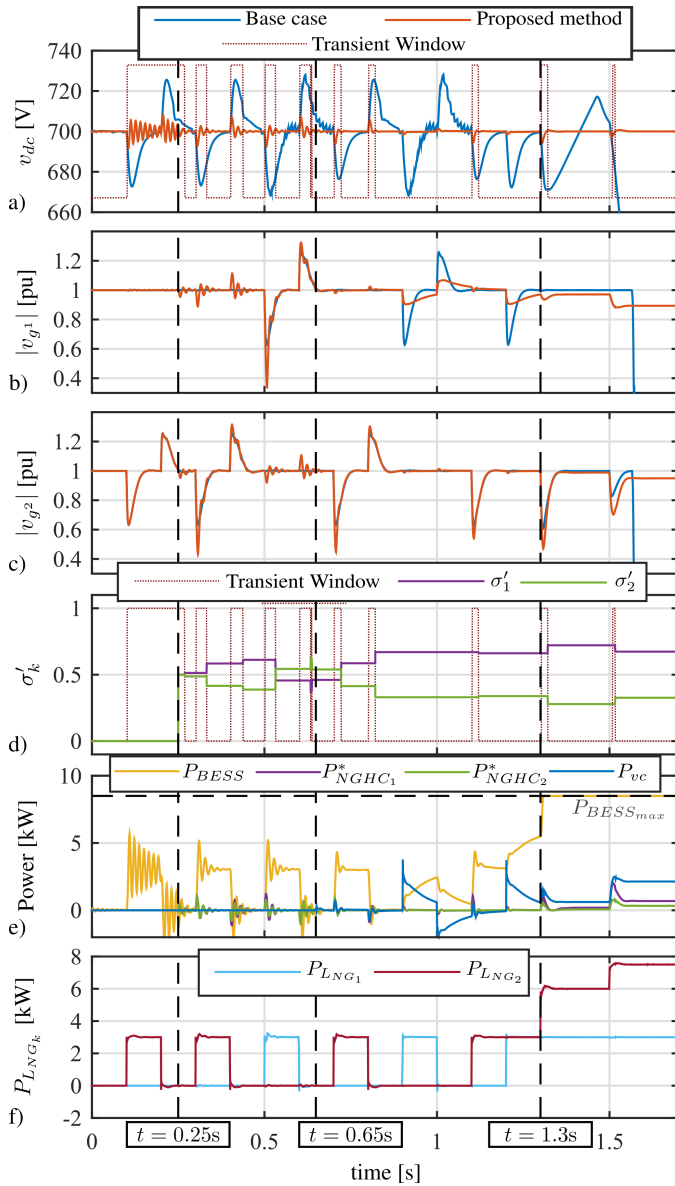


Fig. 11. Simulation results: system performance using the proposed methods. a) LVDC Voltage; b)  $NG_1$  voltage magnitude in p.u., c)  $NG_2$  voltage magnitude in p.u., d) transient window obtained by (24), and sharing coefficients, e) Power shared by the elements participating in the active power control, f) Load drawn by the CPLs located in the NGs.

hand, the use of a local compensator not only improves the transients but also enables the sharing mechanism to operate during steady state. Once the BESS limits, the compensator starts to provide power to maintain the DC and AC NGs at the expense of a stationary error in  $V_{g1}$  caused by the P regulator in the local AC voltage compensator.

### B. Experimental Results

The experimental setup follows the scheme in Fig. 1. The NGs are populated as follows: 1) A tightly regulated CPL, that acts as a load profile emulator, has been connected in the node  $B_2^2$  of  $NG_2$ ; 2) A voltage compensator supplied by

a BESS has been located at the node  $B_1^1$  of  $NG_1$ . For the sake of simplicity, only this two elements, together with the converters in the transformation center, will be considered in this paper.

The experimental results are summarized in Fig. 12, where the *base case* and the proposed method are compared. It shows the DC voltage, the AC voltage in both NGs in p.u., the sharing coefficients  $\sigma'_k$ , the CPL in  $NG_2$  and the power shared by the voltage compensator in  $NG_1$ . The system is tested under multiple steps of CPL disturbances in  $NG_2$ . The sequence of events are described as follows:

- Between  $t = 0$ s and  $t = 0.8$ s, the proposed sharing technique is enabled while the local AC voltage compensator is inactive. The power required by the DC voltage controller is shared between both NGs and the central BESS, reacting  $NG_1$  to the events on  $NG_2$ . As expected, the DC voltage transients are notably improved compared to the *base case*. However, as a consequence, the voltage in  $NG_1$  is distorted and in  $NG_2$  the transient response might be worsen, depending on the sharing coefficient. Initially,  $\sigma'_1 = \sigma'_2$ , thus the power  $P_{C_{dc,hpf}}^*$  is shared equally by the NGHCs. As the coefficient change, the transient response in the NGs is modified. As in this example the load steps take place only in  $NG_2$ , with the consequent significant voltage deviations, the adaptive sharing algorithm tends to reduce the collaboration of  $NGHC_2$ , increasing the participation of  $NGHC_1$  until a steady value of 0.75. However, as the voltage compensator is disabled, the only element providing inertia, i.e. active power, in  $NG_1$  is the filter capacitor, thus the participation of  $NGHC_1$  negatively impacts the  $NG_1$  AC voltage.
- At  $t = 0.8$ s, a local voltage compensator in  $NG_1$  is activated providing additional inertia, leading to an overall improvement in both DC and AC voltages as shown before in the simulation results. As soon as the  $NG_1$  voltage profile is improved due to the compensator, the adaptive mechanism keeps increasing the participation of  $NGHC_1$  in the LVDC control, alleviating the effort of  $NGHC_2$ . It is worth to point out how the voltage compensator in  $NG_1$  reacts to active power transients taking place in  $NG_2$ . This behavior is allowed by the proposed control scheme based on adaptive power sharing.

## VI. DISTURBANCE TO OUTPUT FREQUENCY RESPONSE

In order to further prove the feasibility of the proposed methods and highlight the achievements against the *base case*, the proposed system has been linearized. Its disturbance to output transfer functions have been analyzed. Two disturbances are considered: the CPL variations in the  $NG_1$ ,  $\Delta P_{L_{NG_1}}$ , and in the  $NG_2$ ,  $\Delta P_{L_{NG_2}}(s)$ . Three outputs are taken into account: the LVDC voltage variation,  $\Delta V_{dc}$ , and the NGs voltage magnitude variation,  $\Delta |V_{g1}|$  and  $\Delta |V_{g2}|$ .

Fig. 13 shows the Bode diagrams of those transfer functions for 3 different cases: 1) the *base case*; 2) proposed adaptive

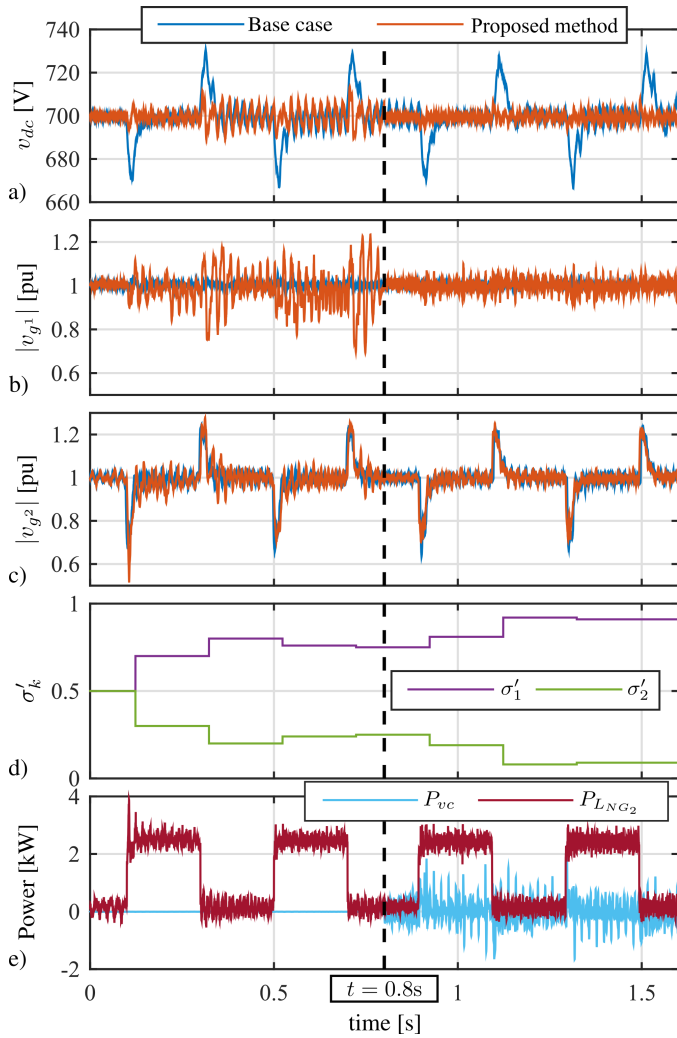


Fig. 12. Experimental results: system performance using the proposed methods. a) LVDC Voltage; b)  $NG_1$  voltage magnitude in p.u., c)  $NG_2$  voltage magnitude in p.u., d) sharing coefficients, e) Load drawn by the CPL located in the  $NG_2$  and power shared by the voltage compensator.

sharing method without local compensators, 3) proposed adaptive method with a local voltage compensator in the  $NG_1$ . Those 3 cases have been evaluated in 3 equilibrium points ( $t = 0.09s$ ,  $t = 0.29$  and  $t = 0.89$  respectively) of the simulated system in Fig. 11. The Bode plots are explained as follows:

- a) & d): As the proposed adaptive method (red) allows to increase the bandwidth of the DC voltage controller, the response is clearly improved at low and medium frequencies. In addition, when the voltage compensator is included (yellow), the response is further enhanced, specially in medium frequencies. It is worth noting that, although the local compensator is in  $NG_1$ , the response under  $\Delta P_{LNG_2}$  is also improved thanks to the indirect cooperation between NGs.
- b) & f): Here, the counter part of the power sharing mechanism (red) is shown. In order to improve the overall system operating range and the DC profile, the

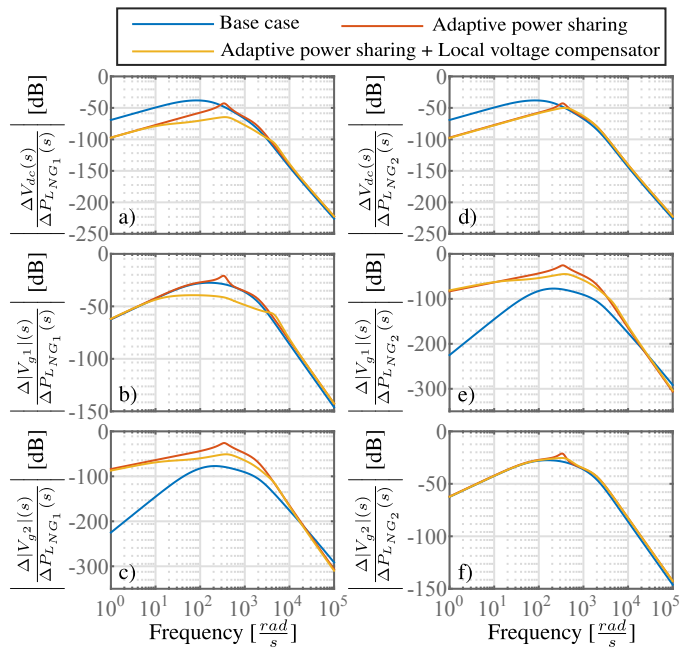


Fig. 13. Bode diagram of the disturbance to output voltage transfer functions. The *base case* and the proposed methods are compared. a), b) and c) voltage variation in the LVDC and the NGs ( $\Delta V_{dc}$ ,  $\Delta |V_{g1}|$ ,  $\Delta |V_{g2}|$ ) under a CPLs disturbance in the  $NG_1$ . d), e) and f) voltage variation in the LVDC and the NGs ( $\Delta V_{dc}$ ,  $\Delta |V_{g1}|$ ,  $\Delta |V_{g2}|$ ) under a CPLs in the  $NG_2$ .

NGs disturbance rejection is slightly worsen. However, the local compensator (yellow) attenuates this effect in f) ( $NG_2$ ), and improves drastically the response in b) ( $NG_1$ ) against the *base case*.

- c) & e): In the *base case* (blue) the two NGs are decoupled from each other, thus  $\Delta P_{LNG_2}$  has a negligible effect in the  $NG_1$  and vice-versa (their coupling is mainly due to sensor errors and delays). The adaptive sharing method allows to couple both NGs increasing the cross-effect that one has on the other as shown in c) and e). This enables the collaborative power flow between NGs.

The gain margins of the transfer functions represented in Fig. 13 are listed in Table II, where a) to f) refers to each Bode plot. The difference between the proposed methods and the *base case* are included below the gain margins. As shown, by slightly compromising the margins in b) and f), a noticeable improvement appears in the DC link a). In the case of the cross-effect transfer functions c) and e), the gain margins are still higher than in b) and f). It is worth pointing out that in every case the phase margin is infinite and the gain margin is positive, ensuring the global stability in all the analyzed cases.

## VII. CONCLUSIONS

In this paper, a dynamic voltage control technique is proposed for a fixed frequency hybrid AC/DC Microgrid with ESSs, based on the power sharing between the AC NGs and a central BESS to maintain the grid quality in both the LVDC and the AC NGs and increase the flexibility under high penetration of CPLs and PECs. An adaptive power sharing

TABLE II  
 GAIN MARGINS FOR THE TRANSFER FUNCTIONS IN FIG. 13.

Gain margins [dB]	$\Delta P_{L_{NG1}}$ disturbance			$\Delta P_{L_{NG2}}$ disturbance		
	$\Delta V_{dc}$ a)	$\Delta  V_{g1} $ b)	$\Delta  V_{g2} $ c)	$\Delta V_{dc}$ d)	$\Delta  V_{g1} $ e)	$\Delta  V_{g2} $ f)
Base case	38.5	27.6	77.2	38.5	77.2	27.5
Adaptive	46.9	24.9	30.9	46.9	30.5	25.2
Adaptive & comp.	67.2	39.4	54.9	52.4	48.8	26.4
Adaptive vs. base case	8.4	-2.7	-46.3	8.4	-46.7	-2.3
Adaptive & comp. vs. base case	27.6	11.8	-22.3	13.9	-28.4	-1.1

mechanism have being presented for maintaining the LVDC voltage under control, not only reducing the stress in the central BESS system and the dependence in the utility grid, but also demonstrating the extended operation and improved transient response in the LVDC when the central BESS presents bandwidth and power limitations. An automatic cooperative sharing method for the power exchanged between the AC NGs have been proposed. Its operation, together with the use of a local AC dynamic voltage compensator based on a virtual capacitance, positively affects the operation of the Microgrid. The theoretical discussion has been supported with simulations, experimental results and a study on the system frequency response.

#### REFERENCES

[1] J. M. Guerrero, "Editorial Special Issue on Power Electronics for Microgrids 2014;Part II," *IEEE Transactions on Power Electronics*, vol. 26, no. 3, pp. 659–663, March 2011.

[2] J. Guerrero, P. C. Loh, T.-L. Lee, and M. Chandorkar, "Advanced Control Architectures for Intelligent Microgrids 2014;Part II: Power Quality, Energy Storage, and AC/DC Microgrids," *IEEE Transactions on Industrial Electronics*, vol. 60, no. 4, pp. 1263–1270, April 2013.

[3] P. Wang, X. Liu, C. Jin, P. Loh, and F. Choo, "A hybrid AC/DC microgrid architecture, operation and control," in *Power and Energy Society General Meeting, 2011 IEEE*, July 2011, pp. 1–8.

[4] J. Zhang, D. Guo, F. Wang, Y. Zuo, and H. Zhang, "Control strategy of interlinking converter in hybrid AC/DC microgrid," in *Renewable Energy Research and Applications (ICRERA), 2013 International Conference on*, Oct 2013, pp. 97–102.

[5] E. Unamuno and J. A. Barrena, "Hybrid ac/dc microgridspart i: Review and classification of topologies," *Renewable and Sustainable Energy Reviews*, vol. 52, pp. 1251 – 1259, 2015. [Online]. Available: <http://www.sciencedirect.com/science/article/pii/S1364032115008412>

[6] M. Ambia, A. Al-Durra, and S. Mueen, "Centralized power control strategy for AC-DC hybrid micro-grid system using multi-converter scheme," in *IECON 2011 - 37th Annual Conference on IEEE Industrial Electronics Society*, Nov 2011, pp. 843–848.

[7] X. Zhou, Y. Chen, L. Zhou, A. Luo, J. M. Guerrero, W. Wu, L. Yang, and W. Tan, "Power coordinated control method with frequency support capability for hybrid single/three-phase microgrid," *IET Generation, Transmission Distribution*, vol. 12, no. 10, pp. 2397–2405, 2018.

[8] P. Garca, P. Arbolea, B. Mohamed, and A. A. C. Vega, "Implementation of a hybrid distributed/centralized real-time monitoring system for a dc/ac microgrid with energy storage capabilities," *IEEE Transactions on Industrial Informatics*, vol. 12, no. 5, pp. 1900–1909, Oct 2016.

[9] Y.-R. Mohamed and E. El-Saadany, "Adaptive Decentralized Droop Controller to Preserve Power Sharing Stability of Paralleled Inverters in Distributed Generation Microgrids," *Power Electronics, IEEE Transactions on*, vol. 23, no. 6, pp. 2806–2816, Nov 2008.

[10] M. Golsorkhi and D. Lu, "A Control Method for Inverter-Based Islanded Microgrids Based on V-I Droop Characteristics," *Power Delivery, IEEE Transactions on*, vol. 30, no. 3, pp. 1196–1204, June 2015.

[11] P. Arbolea, C. Gonzalez-Moran, and M. Coto, "A hybrid central-distributed control applied to microgrids with droop characteristic based generators," in *Power Electronics and Motion Control Conference (EPE/PEMC), 2012 15th International*, Sept 2012, pp. L57a.5–1–L57a.5–8.

[12] T. Dragievi, X. Lu, J. C. Vasquez, and J. M. Guerrero, "DC Microgrids-Part I: A Review of Control Strategies and Stabilization Techniques," *IEEE Transactions on Power Electronics*, vol. 31, no. 7, pp. 4876–4891, July 2016.

[13] D. Chen and L. Xu, "Autonomous dc voltage control of a dc microgrid with multiple slack terminals," *IEEE Transactions on Power Systems*, vol. 27, no. 4, pp. 1897–1905, Nov 2012.

[14] E. Unamuno and J. A. Barrena, "Hybrid ac/dc microgridspart ii: Review and classification of control strategies," *Renewable and Sustainable Energy Reviews*, vol. 52, pp. 1123 – 1134, 2015. [Online]. Available: <http://www.sciencedirect.com/science/article/pii/S1364032115008333>

[15] Z. Zhang, X. Huang, J. Jiang, and B. Wu, "A load-sharing control scheme for a microgrid with a fixed frequency inverter," *Electric Power Systems Research*, vol. 80, no. 3, pp. 311 – 317, 2010.

[16] L. Benadero, R. Cristiano, D. J. Pagano, and E. Ponce, "Nonlinear analysis of interconnected power converters: A case study," *IEEE Journal on Emerging and Selected Topics in Circuits and Systems*, vol. 5, no. 3, pp. 326–335, Sept 2015.

[17] T. Vandoom, B. Renders, L. Degroote, B. Meersman, and L. Vandeveldel, "Active Load Control in Islanded Microgrids Based on the Grid Voltage," *Smart Grid, IEEE Transactions on*, vol. 2, no. 1, pp. 139–151, March 2011, use of Voltage-droop control.

[18] A. Navarro-Rodriguez, P. Garcia, R. Georgious, and J. Garcia, "A communication-less solution for transient frequency drift compensation on weak microgrids using a D-statcom with an energy storage system," in *Energy Conversion Congress and Exposition (ECCE), 2015 IEEE*, Sept 2015, pp. 6904–6911.

[19] I. Serban and C. Marinescu, "Control Strategy of Three-Phase Battery Energy Storage Systems for Frequency Support in Microgrids and with Uninterrupted Supply of Local Loads," *Power Electronics, IEEE Transactions on*, vol. 29, no. 9, pp. 5010–5020, Sept 2014.

[20] M. Torres L, L. Lopes, L. Moran T, and J. Espinoza C, "Self-Tuning Virtual Synchronous Machine: A Control Strategy for Energy Storage Systems to Support Dynamic Frequency Control," *Energy Conversion, IEEE Transactions on*, vol. 29, no. 4, pp. 833–840, Dec 2014.

[21] Y. Hirase, O. Noro, K. Sugimoto, K. Sakimoto, Y. Shindo, and T. Ise, "Effects of suppressing frequency fluctuations by parallel operation of virtual synchronous generator in microgrids," in *Energy Conversion Congress and Exposition (ECCE), 2015 IEEE*, Sept 2015, pp. 3694–3701.

[22] A. Navarro-Rodriguez, P. Garcia, R. Georgious, J. Garcia, and S. Saeed, "Observer-based transient frequency drift compensation in ac microgrids," *IEEE Transactions on Smart Grid*, vol. PP, no. 99, pp. 1–1, 2017.

[23] A. Navarro-Rodriguez, P. Garcia, J. M. Cano, and M. Sumner, "Limits, stability and disturbance rejection analysis of voltage control loop strategies for grid forming converters in dc and ac microgrids with high penetration of constant power loads," in *2017 19th European Conference on Power Electronics and Applications (EPE'17 ECCE Europe)*, Sept 2017, pp. P.1–P.10.

[24] A. Navarro-Rodriguez, P. Garcia, R. Georgious, and J. Garcia, "Adaptive active power sharing techniques for DC and AC voltage control in a hybrid DC/AC microgrid," in *2017 IEEE Energy Conversion Congress and Exposition (ECCE)*, Oct 2017, pp. 30–36.

[25] M. K. Mishra and K. Karthikeyan, "A fast-acting dc-link voltage controller for three-phase dstatcom to compensate ac and dc loads," *IEEE Transactions on Power Delivery*, vol. 24, no. 4, pp. 2291–2299, Oct 2009.

[26] S. Vazquez, J. A. Sanchez, J. M. Carrasco, J. I. Leon, and E. Galvan, "A model-based direct power control for three-phase power converters," *IEEE Transactions on Industrial Electronics*, vol. 55, no. 4, pp. 1647–1657, April 2008.



**Ángel Navarro-Rodríguez** (S'15) received the B.Sc. degree in telecommunications engineering with honors from the University of Castilla La-Mancha, Spain in 2012 and the M.Sc. degree in Electrical Energy Conversion and Power Systems from the University of Oviedo, Gijón, Spain in 2014. Nowadays he is Ph.D student in the Department of Electrical, Computer, and Systems Engineering in the University of Oviedo, granted by the government of Principado de Asturias. In 2016 and 2017, he was a visitor researcher at The University of Nottingham,

UK, in the Power Electronics, Machines and Control (PEMC) research group. He is part of the LEMUR research group in University of Oviedo since 2014 and his research interests include Energy Storage Systems, Control Systems, Electronics, Power Electronic Converters, Microgrids, power quality and Renewable Energies.



**Pablo García** (S01-A06-M09) received the M.S. and Ph.D. degrees in electrical engineering and control from the University of Oviedo, Gijón, Spain, in 2001 and 2006, respectively. In 2004, he was a Visitor Scholar at the University of Madison-Wisconsin, Madison, WI, USA, Electric Machines and Power Electronics Consortium. In 2013 he was a visiting scholar at The University of Nottingham, UK. He is the co-author of more than 20 IEEE journals and 50 international conferences. He is currently an Associate Professor within the Department of

Electrical, Electronics, Computer, and Systems Engineering at the University of Oviedo. His research interests include control of grid-tied converters, parameter estimation, energy conversion, AC drives, sensorless control, AC machines diagnostics and signal processing.



**Ramy Georgious** (S'15) received the B.Sc. degree from Port Said University, Port Said, Egypt, in May 2010, in Electrical Engineering with average appreciation Excellent with honors degree, and the M.Sc. degree in Electrical Energy Conversion and Power Systems (EECPs) and the Ph.D. degree in electrical engineering from the University of Oviedo, Gijón, Asturias, Spain, in June 2014 and July 2018, respectively. He worked as a teacher assistant in the Electrical Engineering department in Port Said University from March 2011 to September 2012. He

joined LEMUR research team in University of Oviedo in July 2014. In 2015, he was a visitor researcher with Power Electronics, Machines and Control (PEMC) research group at the University of Nottingham, United Kingdom. He was granted by Erasmus Mundus (MEDASTAR) to do his Master in 2012 and by the government of Principado de Asturias to do his Ph.D. in 2013 in the University of Oviedo. His research interests include Energy Storage Systems, Control Systems, Power Electronic Converters, Microgrids, Renewable Energy, Design and Simulation.



**Jorge García** (S'01-M'05-SM'11), received the M.Sc. and Ph.D. degrees in electrical engineering from the University of Oviedo, Asturias, Spain, in 2000 and 2003, respectively. In December 1999, he joined the Electrical and Electronic Engineering Department of the University of Oviedo, where he is currently an Associate Professor. He works with the LEMUR research team; his current research interests include power electronics and control for industrial, grid support and lighting applications. Dr. García is co-author of more than 40 journal papers and more

than 80 international conference papers in power and industrial electronics. Dr. García was a recipient of the University of Oviedo Outstanding Ph.D. Thesis Award in 2005.